Proceedings of IMECE2005
2005 ASME International Mechanical Engineering Congress and Exposition
November 5-11, 2005, Orlando, Florida USA

IMECE2005-81967

ADAPTIVE ROBUST REPETITIVE CONTROL OF PIEZOELECTRIC ACTUATORS

Jinghua Zhong
Intelligent and Precision Control Laboratory
School of Mechanical Engineering
Purdue University
West Lafayette, Indiana 47907
Email: jzhong@purdue.edu

Bin Yao*
Intelligent and Precision Control Laboratory
School of Mechanical Engineering
Purdue University
West Lafayette, Indiana 47907
Email: byao@purdue.edu

ABSTRACT

Positioning stages using piezoelectric stack actuators (PEA) possess very high theoretical bandwidth and resolution. However, their tracking performance deteriorates as nonlinear dynamics due to inherent hysteresis starts to dominate when the total length of travel increases. When tracking periodic trajectories, which is common in most industrial applications, the uncertain nonlinearity from hysteresis also becomes periodic. Having identified and separated the fast and slow dynamics of the total stage response, we adopt a simple first-order model assuming the inertial dynamics of the stage is negligible in the low tracking frequency range. By approximating the hysteresis mapping function with simple functions, the overall system model is linearly parameterized for subsequent adaptive robust controller design. Exploiting the periodicity of the uncertain hysteresis nonlinearity, it is further parameterized as finite series of harmonic functions, which eliminates the need for an exact inversion model for hysteresis while achieving high tracking accuracy. Experimental results from tracking control of sinusoidal and typical triangular trajectories show tracking error close to the sensor noise level and demonstrate the effectiveness of the approach.

INTRODUCTION

Positioning stages for high-precision positioning and tracking applications, especially atomic force microscopy that requires resolution on the nanometer level, almost unanimously use piezoelectric actuators, because they are capable of producing sub-nanometer displacements due to the inverse piezoelectric coupling effect. And they are also capable of generating large forces, which deliver very high bandwidth when fitted with low-inertia platform and high-stiffness flexures in typical positioning mechanisms [1].

When driven at small strain levels, the dynamics of piezoelectric actuators can be described by the classical equation of linear piezoelectricity [2]. However, as the demand for range and driving frequency increases for today's applications, we are faced with major nonlinearity inherent in piezoelectric materials, in particular hysteresis, which typically results from ferroelectric phase transitions in most actuators made of lead zirconate titanate ceramics (PZT). It leads to severe positioning errors if not properly modeled and compensated.

To compensate the hysteresis effect and achieve higher positioning accuracy, various schemes have been proposed, most of which employ both model-based feedforward and robust feedback control. For quasi-static or low frequency applications, the classic Preisach model is a popular choice for feedforward compensation, which approximates the hysteresis with a set of simple relay operators [3,4]. Despite their success, the large set of operator parameters necessary for higher accuracy makes it difficult to identify and implement online. The classic Preisach model is also invalid for faster operations unless certain dynamic extensions are made, but the inversion of existing dynamic Preisach models are known to be difficult [5]. In addition, due to the loading history dependence of the hysteresis, the actuator often starts from an unknown initial state that differs from the one under which the parameters were measured offline. Thus a different

*Address all correspondence to this author.

approach with less parameters and easy to adapt on-line is needed for better tracking.

The difficulty for perfect tracking is much reduced when the desired trajectory is repetitive. When a piezoelectric actuator is driven by a periodic input, it converges to a steady-state hysteresis loop after a certain number of cycles, a phenomenon commonly known as "accommodation" [5]. Therefore for periodic trajectories, the required input is highly periodic after the first few periods. The input can thus be obtained by methods such as iterative learning control (ILC), which updates the input signal using the error signal from the previous period and avoids inverting complex nonlinear models. This has been shown to achieve exact tracking for a piezoelectric positioner in [6], but the convergence of their method is guaranteed only for trajectories that satisfy the classic Preisach model, which are slow or pseudo-static trajectories. Though easy to implement, such a method require large computer memory and are sensitive to noise because the physical dependence of the unknown nonlinearity over the same period is completely overlooked. The known dynamics of the system is also hard to be incorporated. The tracking error in [6] starts from 100% of the total travel and slowly converges to zero after about 50 periods. This may be too long for real world applications.

A simple remedy to this problem for repetitive control is proposed by Xu and Yao in [7]. By recognising the physical dependence of the values of periodic uncertainties over the same period and using certain known basis functions to capture such dependence, only the amplitudes of the basis functions are needed for parameterization, which can be easily adapted online. It also overcomes the sensitivity to noise because the basis functions naturally smooths out the effect of random noises. Incorporated with the adaptive robust control (ARC) scheme, it guarantees good transient performance, fast convergence, and perfect tracking when enough number of basis functions are used to parameterize the uncertain nonlinearity.

In this paper, we use a simple first order model that describes the dominant relaxation dynamics of the hysteretic response for a piezoelectric stage with negligible inertial dynamics in our desired range of operation. The adaptive robust repetitive control scheme mentioned above is applied to the model, which adapts the unknown parameters using a discontinuous projection based method, and the uncompensated nonlinearities are attenuated by certain robust control laws. No exact model of the hysteresis is needed, and the steady-state tracking error is reduced to almost the sensor noise level for sinusoidal trajectories up to 100 Hz and pseudo-triangular (with smoothed turnaround points) trajectories up to 50 Hz. Transient error is less than 3 percent of the total length and convergence happens within 2 periods, demonstrating the effectiveness of the method.

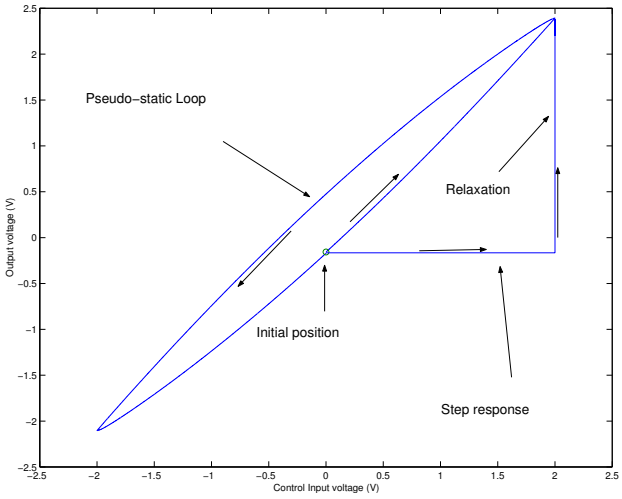

Figure 1. Open-loop system response to 0.1V/s 4Vpp triangular input and a 2-volt step, both starting from the same initial position and loading history.

MODELING OF THE PIEZOELECTRIC STAGE SYSTEM

The Positioning Stage System

The system to be controlled is a commercially available nano-positioning stage driven by a piezoelectric stack actuator with an integrated capacitive position sensor (Polytec PI P753.11C). The unit has a total travel of 12 μm, which corresponds to an applied voltage range of 0-100 volts. To avoid possible saturation in the driving amplifier, we limit our range of interest to about 2.4μm (0-2V of the sensor output). At this range, the actuator already exhibits very noticeable hysteresis. Figure 1 shows the response of the actuator to a pseudo-static (0.1volt/sec) 4 volt peak-to-peak triangular input. For convenience, the sensor output voltage is used for the dimension of displacement throughout the paper.

Identification of the Plant Model

The total response of the stage consists of two components: a fast response due to elastic displacement of the piezoelectric material that dominates the dynamics in the short travel and range, and a hysteretic response due to dipole domain switching, which resembles a nonlinear relaxation process [5, 8].

Inertial Dynamics of the Stage The bode plot for the inertial dynamics of the stage has previously been identified using a sinusoidal sweep excitation signal from $0 - 12.8$kHz [8]. The amplitude of the excitation signal is restricted to a maximum of 30mV to avoid distortion from hysteresis as much as possible. Different offsets (-1,0,2,3 V) has been added to the input signal and the bode plots remain almost identical, implying the linear

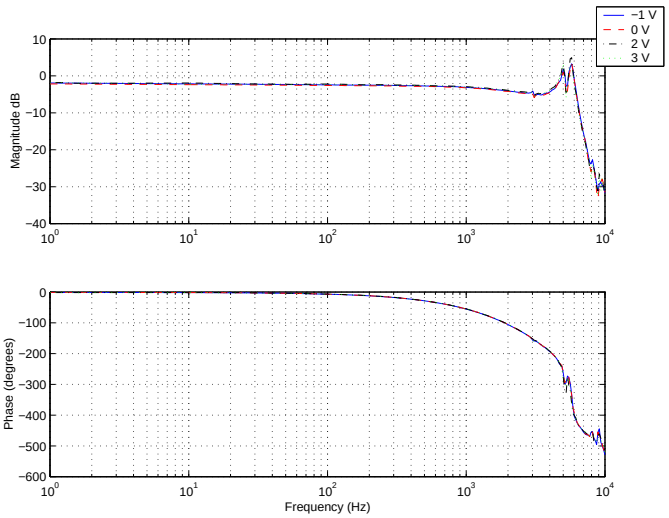

Figure 2. Low excitation frequency response of the stage at different offsets of the excitation signal.

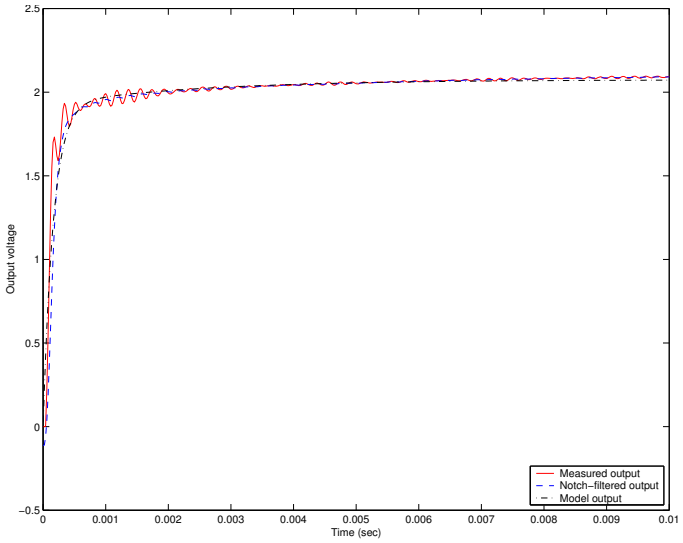

Figure 3. 2V step response of the stage in the first 0.01 seconds.

nature of this dynamics (Figure 2). The stage has two resonance peaks at about 5100 and 5800 kHz. Below 500Hz, there is negligible phase delay and the gain stays almost constant. Therefore, for operation frequencies in this range, it is safe to assume the inertial dynamics is negligible and can be represented by an uncertain constant gain. To be conservative, we limit our close-loop bandwidth to 200Hz and our desired trajectories to 100Hz.

Relaxation Dynamics The pseudo-static response curve shown in Figure 1 is measured after carefully driving the stage to a full-range loop that returns from its lowest displacement at -2 volt. If further input voltage does not exceed the [-2v, 2v] range, the system always relaxes to a point within this loop when the input is held constant. To identify the relaxation dynamics, a 2-volt step input is applied to the system after carefully initializing the actuator to the same starting position on the loop. It is observed that response is very quick at the beginning, and then slowly relaxes to a steady-state value of 2.45 volts, which coincides with the corresponding displacement on the pseudo-static loop at the same input voltage.

Figure 3 shows the 2-volt step response in time domain during the first 0.01 seconds. After filtering out the resonance from the inertial dynamics and accounting for time-delays, we are able to fit the relaxation response using two first-order transfer function in parallel, whose time constants are about 0.1 and 2 ms. The bandwidth of the faster response is 2 orders of magnitude higher than our desired bandwidth, therefore it is modeled as a simple gain. The slower response thus becomes the only dominant dynamics of the system. Combining this dynamics with the instantaneous gain, the overall model is reduced to a simple first order system

$$\begin{aligned} \tau \dot{x}_h &= -x_h + b_1 g_t(u), \\ y &= x_h + b_0 g_t(u), \end{aligned} \tag{1}$$

where $g_t(u)$ is a function that maps the input u to the steady-state output of the system, which is hysteretic and history dependent, b_0 is the feed-through gain and b_1 is the input gain for the first order dynamics. Notice that $b_0 + b_1 = 1$, because the output y should converge to $g_t(u)$ at steady state.

ADAPTIVE ROBUST REPETITIVE CONTROL OF PIEZOELECTRIC ACTUATORS

Design Model and Assumptions

The hysteresis mapping function $g_t(u)$ in (1) can not be easily represented with simple functions, as it essentially describes the internal state of dipole domains and thus depends on the past history of actuator displacement. Since our desired trajectory is periodic, the hysteresis nonlinearity also becomes periodic, so an exact model is less critical for tracking control. Therefore, we use an approximate linear relationship and leave the uncertain discrepancy to online adaptation. Replacing $g_t(u)$ by the simple linear function

$$g_t(u) = k_u u + d_g(t), \tag{2}$$

which is a straight line, the system equations are further simplified to

$$\begin{aligned} \tau \dot{x}_h &= -x_h + b_1[k_u u + d_g(t)], \\ y &= x_h + b_0[k_u u + d_g(t)]. \end{aligned} \tag{3}$$

The discrepancy term $d_g(t)$ of the linear relationship represents the time-varying mismatch between $k_u u$ and $g_t(u)$. The parameter k_u captures the average slope of the hysteresis loop that covers the entire range of desired operation, so it depends on the desired length of travel and prior displacement. In this paper, since the actuator output is always below 2 volts, the curve $g_t(u)$ is always contained within the pseudo-static loop shown in Figure 1. The initial estimate and possible range for k_u and $d_g(t)$ is thus easy to obtain from experiments.

Defining the system state vector $[x_1, x_2]^T = [y, u]^T$ and using $v = \dot{u}$ as a virtual input (also noting the identity $b_0 + b_1 = 1$), we may rewrite (3) as

$$\begin{aligned} \frac{1}{b_0 k_u}\dot{x}_1 &= -\frac{1}{\tau b_0 k_u}x_1 + \frac{1}{\tau b_0}x_2 + \frac{1}{k_u}[\frac{1}{\tau b_0}d_g + \dot{d}_g] + v, \\ \dot{x}_2 &= v, \\ y &= x_1. \end{aligned} \tag{4}$$

The term $\frac{1}{k_u}[\frac{1}{\tau b_0}d_g + \dot{d}_g]$, representing the uncertain nonlinearity from hysteresis, is highly periodic with a known period T. It can be represented by a finite Fourier series

$$\begin{aligned} \frac{1}{k_u}[\frac{1}{\tau b_0}d_g + \dot{d}_g] &= \frac{A_0}{2} + \sum_{n=1}^{m}(A_n \cos n\omega t + B_n \sin n\omega t) + \Delta \\ &= \Phi_d^T \theta_d + \Delta, \end{aligned} \tag{5}$$

where $\theta_d = [A_0/2, A_1, B_1, \cdots, A_m, B_m]^T$ represent the unknown Fourier coefficients, $\Phi_d^T = [1, \cos\omega t, \sin\omega t, \cdots, \cos m\omega t, \sin m\omega t]$ are the basis functions, and Δ is the unknown variation between the series and the true nonlinearity. Since the mechanical system has finite bandwidth, the first few terms will be enough for a good approximation in practice.

To use parameter adaptation, we define the unknown parameter set $\theta^T = [\theta_1, \theta_2, \theta_3, \theta_d^T]$ with $\theta_1 = \frac{1}{b_0 k_u}$, $\theta_2 = \frac{1}{\tau b_0 k_u}$, and $\theta_3 = \frac{1}{\tau b_0}$. The state space equation (4) is now linearly parameterized in terms of θ as

$$\theta_1 \dot{x}_1 = -\theta_2 x_1 + \theta_3 x_2 + \Phi_d^T \theta_d + \Delta + v, \tag{6}$$

$$\dot{x}_2 = v. \tag{7}$$

We can make the following reasonable and practical assumption on the parameters [9]:

Assumption 1. *The extent of parametric uncertainties and uncertain nonlinearities is known, i.e.,*

$$\begin{aligned} \theta &\in \Omega_\theta \triangleq \{\theta :\ \theta_{\min} < \theta < \theta_{\max}\}, \\ \Delta &\in \Omega\Delta \triangleq \{\Delta\ \|\Delta(x,t)\| \le \delta(x,t)\}, \end{aligned} \tag{8}$$

where $\theta_{\min}$, $\theta_{\max}$, and $\delta(x,t)$ are known.

Under Assumption 1, the discontinuous projection based ARC design is applied to (3) to solve the robust tracking control problem. Specifically, the parameter estimation $\hat{\theta}$ is updated through a parameter adaptation law of the form

$$\dot{\hat{\theta}} = \mathrm{Proj}_{\hat{\theta}}(\Gamma\tau) \tag{9}$$

where Γ is any symmetric positive definite adaptation rate matrix (for simplicity, Γ is assumed to be a diagonal matrix in the sequel), τ is an adaptation function to be specified later, and the projection mapping $\mathrm{Proj}_{\hat{\theta}}(\bullet)$ is defined by [10]

$$\mathrm{Proj}_{\hat{\theta}}(\bullet) = \begin{cases} 0 & \text{if} \begin{cases} \hat{\theta}_i = \hat{\theta}_{\max} & \text{and } \bullet > 0, \text{ or} \\ \hat{\theta}_i = \hat{\theta}_{\min} & \text{and } \bullet < 0; \end{cases} \\ \bullet & \text{otherwise,} \end{cases} \tag{10}$$

which has the following properties:

$$\begin{aligned} &\text{P1. } \hat{\theta} \in \bar{\Omega}_\theta = \{\hat{\theta} :\ \theta_{\min} < \hat{\theta} < \theta_{\max}\}, \\ &\text{P2. } \tilde{\theta}^T(\Gamma^{-1}\mathrm{Proj}_{\hat{\theta}}(\Gamma\bullet) - \bullet) \le 0,\ \forall \bullet. \end{aligned} \tag{11}$$

ARC Controller Design

Defining $e = x_1 - y_d$ as the tracking error, the error dynamics of the system becomes

$$\begin{aligned} \theta_1 \dot{e} &= \theta_1 \dot{x}_1 - \theta_1 \dot{y}_d \\ &= -\theta_1 \dot{y}_d - \theta_2 x_1 + \theta_3 x_2 + \Phi_d^T \theta_d + \Delta + v \\ &= \varphi^T \theta + \Delta + v, \end{aligned} \tag{12}$$

where $\varphi^T = [-\dot{y}_d, -x_1, x_2, \Phi_d^T]$. The following ARC control law is proposed, which consists of two parts given by

$$\begin{aligned} v = v_a + v_s,\ v_a = -\varphi^T\hat{\theta}, \\ v_s = v_{s_1} + v_{s_2},\ v_{s_1} = -ke, \end{aligned} \tag{13}$$

where v_a is the adjustable model compensation needed for achieving perfect tracking, and v_s is the robust control law consisting of two parts: v_{s_1} is a simple proportional feedback used

to stabilize the nominal system, and v_{s_2} is a robust feedback used to attenuate the effect of model uncertainties, which is required to satisfy the following two constraints

$$\begin{array}{l} \text{C1. } e[-\varphi^T\tilde{\theta}+\Delta(x,t)+v_{s_2}]\le\varepsilon, \\ \text{C2. } v_{s_2}e\le 0, \end{array} \tag{14}$$

where ε is a positive design parameter representing the attenuation level of the model uncertainties. In (14), constraint C1 is used to represent the fact that v_{s_2} is synthesized to dominate the the model uncertainties coming from both parametric uncertainties and unmodeled nonlinearities to achieve the guaranteed attenuation level ε, and the passive-like constraint C2 is imposed to ensure that introducing v_{s_2} does not interfere with the nominal parameter adaptation process. A simple form of v_{s_2} that satisfy (14) is

$$v_{s_2}=-\frac{1}{4\varepsilon}h^2e, \tag{15}$$

where $h\ge\|\theta_{\max}-\theta_{\min}\|\,\|\varphi\|+\delta(x,t)$. It is used in our experimental implementation due to its computational simplicity. The ARC design above has the following advantages:

Theorem 1. *If the adaptation function in (9) is chosen as*

$$\tau=\varphi(x)e, \tag{16}$$

then the ARC law (13) with the parameter adaptation law (9) guarantees that [9, 11]

***A**. In general, all signals are bounded and the tracking error is bounded by*

$$|e|^2\le\exp(-\frac{2k}{\theta_{1max}}t)\frac{2|e(0)|^2}{\theta_1}+\frac{\varepsilon\theta_{1max}}{2k}[1-\exp(-\frac{2k}{\theta_{1max}}t)]. \tag{17}$$

The exponential converging rate $\frac{2k}{\theta_{1max}}$ and the size of the final tracking error ($|e(\infty)|\le\sqrt{\frac{\varepsilon\theta_{1max}}{2k}}$) can be freely adjusted by the controller parameters ε and k in a known form.

***B**. If after a finite time, there exist parametric uncertainties only (i.e., $\Delta(x,t)=0,\forall t\ge t_0$), then in addition to the results in A, zero tracking error is achieved, i.e., $e\to 0$ as $t\to\infty$.*

Proof. Defining a positive definite function $V_s=\frac{1}{2}\theta_1e^2$ and differentiating, also noting constraint C1 of (14), we have

$$\begin{aligned}\dot{V}_s&=\theta_1e\dot{e}\\&=e[-ke+v_s+\Delta-\varphi^T\tilde{\theta}]\\&\le -ke^2+\varepsilon\\&\le -\frac{2k}{\theta_{1max}}V_s+\varepsilon,\end{aligned} \tag{18}$$

therefore $V_s\le\exp(-\frac{2k}{\theta_{1max}}t)V_s(0)+\frac{\varepsilon\theta_{1max}}{2k}[1-\exp(-\frac{2k}{\theta_{1max}}t)]$. Substituting $|e|^2=\frac{2V_s}{\theta_1}$ back leads to part A.

When $\Delta=0$, define another positive definite function $V_a=\frac{1}{2}\theta_1e^2+\frac{1}{2}\tilde{\theta}^T\Gamma^{-1}\tilde{\theta}$, whose derivative is

$$\begin{aligned}\dot{V}_a&=\theta_1e\dot{e}+\tilde{\theta}^T\Gamma^{-1}\dot{\hat{\theta}}\\&=e[-ke+v_s-\varphi^T\tilde{\theta}]+\tilde{\theta}^T\Gamma^{-1}\dot{\hat{\theta}}.\end{aligned} \tag{19}$$

Noting constraint C2 in (14) and the adaptation function (16), we have

$$\begin{aligned}\dot{V}_a&=-ke^2+v_se+\tilde{\theta}^T(\Gamma^{-1}\dot{\hat{\theta}}-\varphi e)\\&\le -ke^2+\tilde{\theta}^T(\Gamma^{-1}\dot{\hat{\theta}}-\varphi e)\\&=-ke^2+\tilde{\theta}^T(\Gamma^{-1}\mathrm{Proj}_{\hat{\theta}}(\Gamma\varphi e)-\varphi e)\\&\le -ke^2\\&\le 0,\end{aligned} \tag{20}$$

which leads to the asymptotic tracking in part B by easily verifying $\dot{e}\in L_\infty$ and applying Barbalat's Lemma. □

In addition, the system (4) has relative degree one, the internal dynamics for x_2 needs to be BIBO stable for the actual control input to be bounded and implementable. Substituting the ARC law into the internal dynamics (7), we have

$$\dot{x}_2=-\hat{\theta}_3x_2+[\hat{\theta}_1\dot{y}_d+\hat{\theta}_2x_1-\Phi_d^T\hat{\theta}_d-ke-\frac{h^2}{4\varepsilon}e]. \tag{21}$$

Defining a positive definite function $V_2=\frac{1}{2}x_2^2$ and differentiating,

$$\dot{V}_2=x_2\dot{x}_2=-\hat{\theta}_3x_2^2+\left[\hat{\theta}_1\dot{y}_d+\hat{\theta}_2x_1-\Phi_d^T\hat{\theta}_d-ke-\frac{h^2}{4\varepsilon}e\right]x_2. \tag{22}$$

Since all the terms in the square bracket are bounded, we denote the upper bound of the entire term by $\bar{b}$ and also notice that $0<\hat{\theta}_3<\theta_{3min}$, therefore

$$\begin{aligned}\dot{V}_2&\le -\theta_{3min}x_2^2+\bar{b}x_2\\&=-(1-\lambda)\theta_{3min}x_2^2-\lambda\theta_{3min}x_2^2+\bar{b}x_2\\&=-(1-\lambda)\theta_{3min}x_2^2-\lambda\theta_{3min}\left(x_2-\frac{\bar{b}}{2\lambda\theta_{3min}}\right)^2\\&\quad+\frac{\bar{b}^2}{4\lambda\theta_{3min}}\\&\le -(1-\lambda)\theta_{3min}x_2^2+\frac{\bar{b}^2}{4\lambda\theta_{3min}},\end{aligned} \tag{23}$$

where the arbitrary constant $\lambda \in (0,1)$. Equation (23) implies $V_2 \leq V_b(t) = x_2^2(0)e^{-(1-\lambda)\theta_{3min}t} + \frac{\bar{b}^2}{4\lambda\theta_{3min}}[1-(1-\lambda)\theta_{3min}t] \leq x_2^2(0) + \frac{\bar{b}^2}{4\lambda\theta_{3min}}$, therefore $|x_2| = \sqrt{2V_2} \leq \sqrt{2V_b(t)} \leq \sqrt{2x_2^2(0) + \frac{\bar{b}^2}{2\lambda\theta_{3min}}}$ and so x_2 is bounded. □

EXPERIMENTAL RESULTS

Experimental Setup

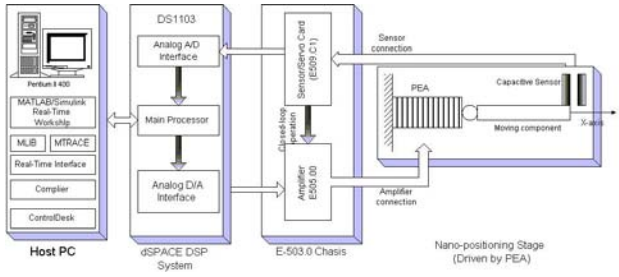

Figure 4. Experimental setup.

As illustrated in Figure 4, the experimental setup of the system consists of four major components: the positioning stage with integrated capacitive displacement sensor, its driving amplifier, a dSPACE DS1103 DSP controller card, and a generic host PC. The base of the stage is screw-mounted on a massive vibration isolation table to minimize induced vibrations in the supporting structure. The signal returned by the capacitive sensor has a maximum noise level of ± 0.0025 volt, which corresponds to ± 3 nm. The driving amplifier (Physik Instrumente E501.00) has an output range of -20 to 120 volts and a bandwidth much higher than required to track the desired frequency range in this paper, so its electrical dynamics is considered negligible.

The driving amplifier can operate in both open-loop and closed-loop modes. In closed-loop mode, the stage is controlled by a built-in PI servo controller. In the open-loop mode, the control voltage signal from the dSPACE card is amplified by a factor of 10 and applied directly to the stage. This mode is used for the experiments.

Controller Parameters

The dSPACE controller board executes the ARC algorithm at a sampling frequency of 10 kHz. We will measure the response to sinusoidal trajectories and triangular trajectories with rounded corners. Since the trajectories are symmetric in one period, only the offset term $A_0/2$ and the odd number harmonics are needed in $\Phi_d^T\theta_d$, so $n = [1,3,5,\cdots]$. In the experiments, using up to $n = 5$ is enough to get the error close to the noise level, so $\Phi_d^T\theta_d$ has 7 terms. The initial values for the parameters are set to $\hat{\theta}(0) = [1.6, 600, 600, 0, 0, 0, 0, 0, 0, 0]^T$. The bounds of the parameter variations are estimated as $\theta_{min} = [0.9, 180, 220, -500, -500, -500, -500, -500, -50, -50]^T$ and $\theta_{max} = [2.4, 2400, 1670, 500, 500, 500, 500, 500, 50, 50]^T$. The magnitude of Δ is assumed to be less than $d_{max} = 500$. The parameters used for the ARC controller are $k_1 = 8000$ and $\varepsilon = 10^{10}$. The adaptation rates are chosen as $\Gamma = \text{diag}\{8, 8\times10^5, 8\times10^5, 2\times10^6, 2\times10^6, 2\times10^6, 2\times10^6, 2\times10^6, 2\times10^6, 2\times10^6\}$.

To reduce transient tracking error, the desired trajectory is generated by filtering the reference trajectory with a second order stable system

$$\ddot{y}_d + 2\zeta\omega_n\dot{y}_d + \omega_n^2 y_d = \ddot{y}_r + 2\zeta\omega_n\dot{y}_r + \omega_n^2 y_r, \qquad (24)$$

with $\zeta = 1$ and $\omega_n = 200\text{Hz} = 400\pi\,\text{rad/sec}$. The initial conditions are set to $y_d(0) = x_1(0)$, $\dot{y}_d(0) = \dot{x}_1(0)$. This is important for the experiments on the piezoelectric stage, because due to hysteresis it is generally difficult to move the stage back to zero position and maintain it without careful input planning before the stage is shut off, so the stage often starts from an undesirable position far from zero when it is first turned on. The filter initialization ensures that the desired trajectory has a quick and smooth transition from the initial position to the reference trajectory.

Tracking Performance

To quantify the performance of our controller, the following performance indices will be used:

(I1) $L_2[e] = \sqrt{\frac{1}{T_f}\int_0^{T_f}|e(t)|^2dt}$, the scalar valued L_2 norm of the tracking error, is used as a measure of *average tracking performance*, where T_f represents the total running time;

(I2) $e_M = \max_t\{|e(t)|\}$, the maximum absolute value of the tracking error, is used as a measure of *transient performance*.

(I3) $e_F = \max_{T_f-2T\leq t\leq T_f}\{|e(t)|\}$, the maximum absolute value of the tracking error during the last 2 periods, is used as a measure of *final tracking accuracy* for periodic trajectories.

Sinusoidal Trajectories. Figure 5 shows the tracking error in the first 10 periods for a 100Hz sinusoidal trajectory $r(t) = 1 - cos(2\pi ft)$[volt], which corresponds to a total travel of 2400nm. The maximum error $e_M = 0.028$volt, which is 1.4% of the total travel. The average error $L_2[e] = 0.0036$volt, which translates to less than 0.2% of the total travel. The final tracking error $e_F = 0.0026$volt is only 0.13% of the total travel and almost the same as the sensor noise level. The estimates of the

4 major parameters (θ_1 through θ_3 and the static component of the harmonic approximation) are shown in Figure 6. The parameters have almost converged after the first period of the sinusoid, despite the fact that the reference trajectory is a simple sinusoid and we have as many as 10 parameters. It is worth noting that the ARC algorithm used in this paper is the so-called direct ARC algorithm, which aims only to reduce tracking error but does not require parameter convergence. The desired trajectory generated from the filter contains not only the reference trajectory but also a decaying part from initial position, increasing the "richness" of the signal in effect.

Figure 7 shows the trend of tracking errors as the number of harmonic functions increases. The transient error is not affected much, as it is determined mostly by the robust feedback gain, but the average error and final tracking error decrease as we increase the highest order of harmonics used to approximate the uncertain nonlinearity.

Pseudo-triangular Trajectories. Figure 8 shows the tracking error in the first 10 periods for a 50 Hz pseudo-triangular trajectory. The constant velocity sections of the trajectory have a length of 2 volts and take 80% of the period. The turn-around points are connected by smooth constant acceleration sections. The first 4 estimated parameters are shown in Figure 9. The tracking performance is not as good as that of sinusoidal trajectory, which is expected because the uncertain nonlinearity when tracking triangular wave would take a lot more harmonics to approximate, but even with the same number of harmonics as before, the final tracking error is already down to 0.0060, or 0.3% of the constant velocity scan length. If more stringent performance is required, more harmonics should be included. The same decreasing trend in error is observed as we increase the highest order of harmonics used, which is shown in Figure 10.

CONCLUSIONS

In this paper, an ARC controller is designed and implemented to control a piezoelectric actuator tracking periodic trajectories at low operating frequencies. By approximating the hysteresis mapping with simple functions and exploiting the periodicity of remaining uncertain nonlinearity when tracking repetitive trajectories, the system model is linearly parameterized for subsequent adaptive robust controller design. Experimental results from tracking control of sinusoidal trajectories up to 100 Hz show tracking error down to the sensor noise level. Tracking error for more useful trajectories such as a 50Hz triangular wave is also at the same magnitude of the noise level. The final tracking error shows a steady decrease as the number of harmonic basis functions increases, demonstrating the effectiveness of the approach.

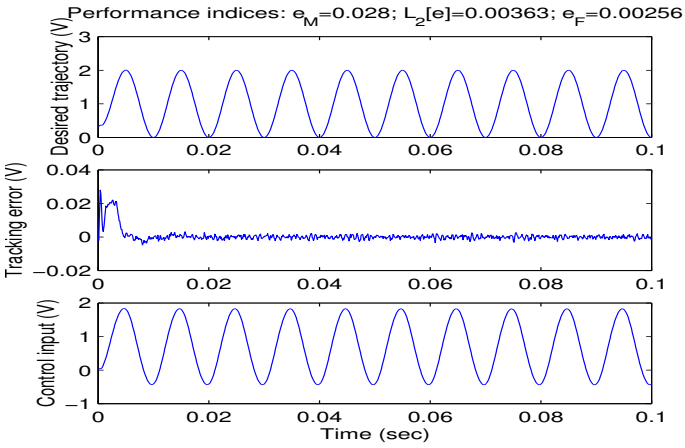

Figure 5. Tracking error for a 100Hz sinusoid.

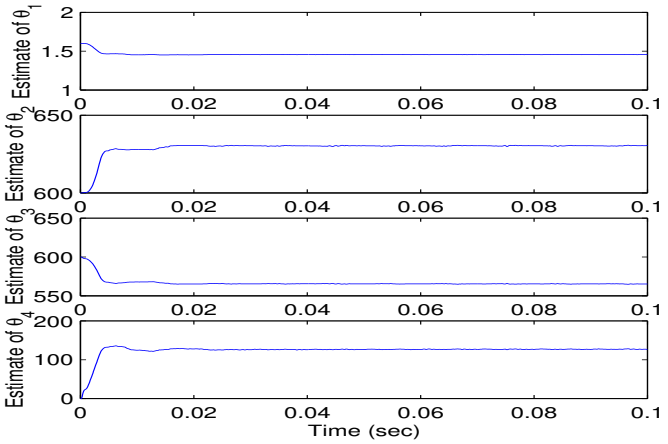

Figure 6. Major parameter estimates for a 100Hz sinusoid.

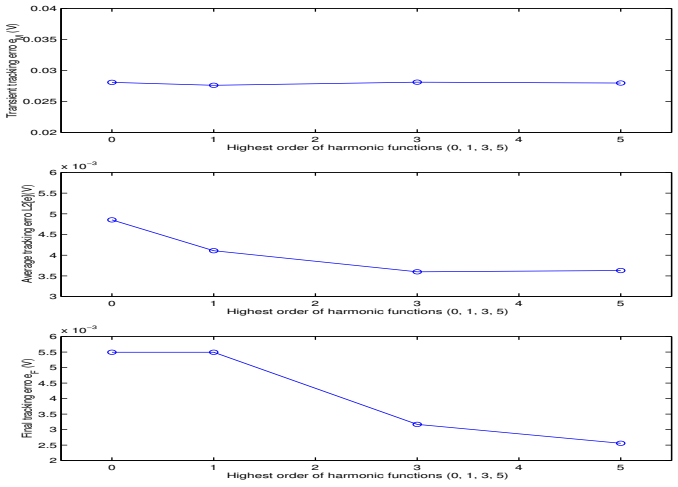

Figure 7. Tracking error v.s. highest order of harmonic functions.

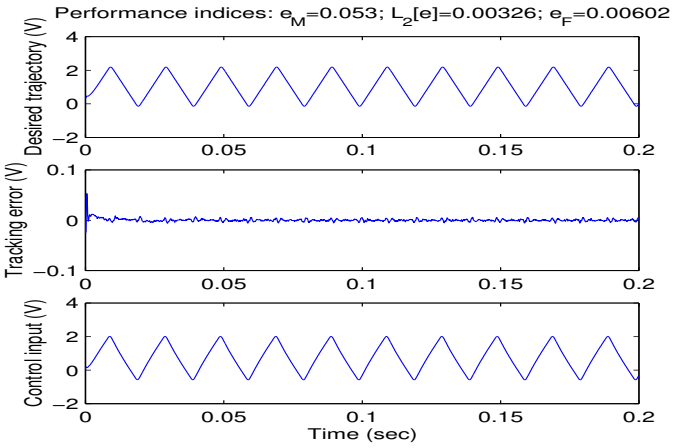

Figure 8. Tracking error for a 50Hz pseudo-triangular trajectory.

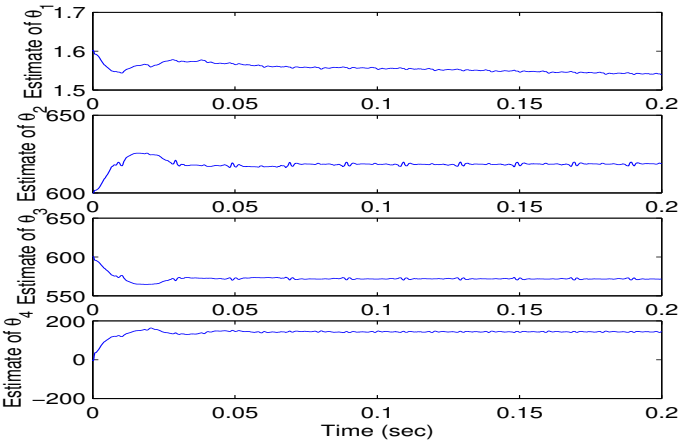

Figure 9. Major parameter estimates.

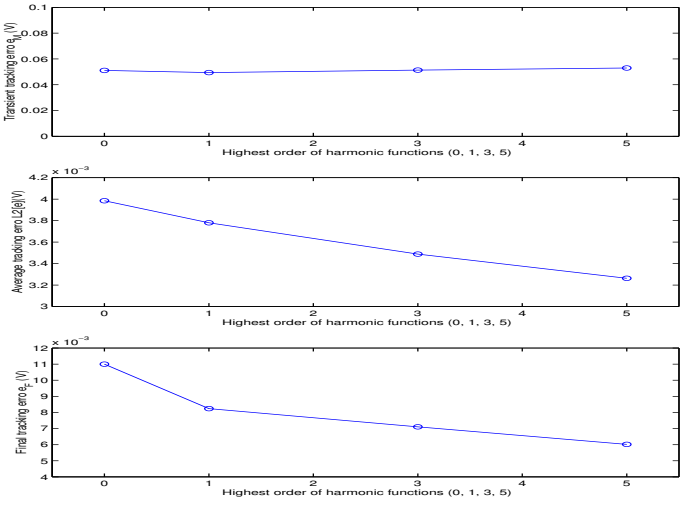

Figure 10. Tracking error v.s. highest order of harmonic functions.

REFERENCES

[1] PhysikInstrumente. http://www.physikinstrumente.com/.

[2] Kamlah, M., and Tsakmakis, C., 1999. "Phenomenological modeling of the non-linear electromechanical coupling in ferroelectrics". *International Journal of Solids and Structures,* **36**, pp. 669–695.

[3] Ge, P., and Jouaneh, M., 1996. "Tracking control of a piezoceramic actuator.". *IEEE Trans. Contr. Syst. Tech.,* **4(3)**, pp. 209–216.

[4] Kuhnen, K., and Janocha, H., 1999. "Adaptive inverse control of piezoelectric actuators with hysteresis operators". In Proceedings of the European Control Conference, Laboratory for Process Automation, University of Saarland, Im Stadtwald, Geb. 13, Saarbrucken Germany; klaus@lpa.uni-sb.de, p. F291.

[5] Mayergoyz, I., 1986. "Mathematical models of hysteresis". In The IEEE Transactions on Magnetics, Vol. MAG-22; No. 5, pp. 603–608.

[6] Leang, K. K., and Devasia, S., 2003. "Iterative feedforward compensation of hysteresis in piezo positioners". In Proceedings of the 42nd IEEE Conference on Decision and Control, pp. 2626–2631.

[7] Yao, B., and Xu, L., 2001. "On the design of adaptive robust repetitive controllers". In ASME International Mechanical Engineering Congress and Exposition (IMECE'01), IMECE01/DSC-3B-4, pp. 1–9.

[8] Ramanujam, R., 2001. "Modelling and control of piezoelectric actuators". Master's thesis, Purdue University, West Lafayette, Indiana, December.

[9] Yao, B., 1997. "High performance adaptive robust control of nonlinear systems: a general framework and new schemes". In Proc. of IEEE Conference on Decision and Control, pp. 2489–2494.

[10] Sastry, S., and Bodson, M., 1989. *Adaptive Control: Stability, Convergence and Robustness*. Prentice Hall, Inc., Englewood Cliffs, NJ 07632, USA.

[11] Yao, B., Jan. 1996. "Adaptive robust control of nonlinear systems with application to control of mechanical systems". PhD thesis, Mechanical Engineering Department, University of California at Berkeley, Berkeley, USA.